A tough and novel dual-response PAA/P(NiPAAM-co-PEGDMA) IPN hydrogels with ceramics by photopolymerization for consolidation of bone fragments following fracture

Gabriel Goetten de Lima [1,2†] , Johanna Katrin Elter [1†] , Bor Shin Chee [1], Washington Luiz Esteves Magalhães [3], Declan M. Devine [1,4], Michael J. D. Nugent [1], Marcelo J.C. de Sá [1,5]

[1] *Materials Research Institute, Athlone Institute of Technology, Athlone, Ireland*

[2] *Integrated Engineering and Materials Sciences Program, Federal University of Paraná, Curitiba, Paraná, Brazil*

[3] *Embrapa Forestry, Colombo, Brazil*

[4] *Rehabilitation Medicine Centre, Mayo Clinic, Rochester, MN, USA*

[5] *Veterinary Hospital, Patos Campus. Federal University of Campina Grande, Paraiba, Brazil.*

[†] These authors contributed equally to this manuscript.

ABSTRACT

In this work, a novel dual-response hydrogel for enhanced bone repair following multiple fractures was investigated. The conventional treatment of multiple bone fracture consists on removing smaller bone fragments from the body in a surgery, followed by the fixation of the bone using screws and plates. This work proposes an alternative for this treatment via *in-situ* UV-initiated radical polymerization of a novel IPN hydrogel composed of PAA/P(NiPAAM-co-PEGDMA) incorporated with ceramic additives. The influence of different additives on mechanical properties and sensitivity of the polymer, as well as the prepolymer mixture, were investigated in order to analyse the suitability of the composites for bone healing applications. This material exhibited an interpenetrating network, confirmed by FTIR, with ceramics particles dispersed in between the polymer network. These structures presented high strength by tensile tests, sensitivity to pH and temperature and a decrease on Tg values of NiPAAm depending on the amount of PEGDMA and ceramics added; although, the addition of ceramics to these composites did not decrease their stability drastically. Finally, cytotoxicity tests revealed variations on the toxicity, whereas the addition of TCP presented to be non-toxic and that the cell viability increased when ceramics additives were incorporated into the polymeric matrix with an increased reporter activity of NF-κB, associated with aiding fibroblast adhesion. Hence, it was possible to optimise feedstock ratios to increase the applicability of the prepolymer mixture as a potential treatment of multiple fractures.

Keywords: composite biomaterials, multiple bone fragment surgery, trauma

1. Introduction

Many materials used in the field of tissue engineering already made their way from the laboratory to an appliance in everyday life. For example, damaged veins, joints or parts of other organs can be replaced or repaired using synthetic materials [1,2]. A drawback in these techniques is often the occurrence of inflammation, as the surrounding natural tissue might not always tolerate the artificial material [3]. Further, the immobilization of the implant is mainly mechanical, that means it has to be screwed or sewed in place before a biological response with this foreign body material occurs [4,5]. However, all implants, including screws and plates, have a passivation phase where leachable ions dissolve out following implantation and could induce a tissue reaction [6].

In this work, biocompatible hydrogels for enhanced bone regeneration after multiple fractures were investigated. Multiple bone fracture can frequently occur in patients with osteoporosis [7], injury assault victims [8] and patients with Fanconi syndrome [9] – some of them due to osteomalacia [10]. Conventionally, the treatment for patients with osteoporosis and osteomalacia, is with the usage of pharmacological agents such as calcium, vitamin D and biphosphanates to prevent further fractures [11]. However, there are no special treatments after the occurrence of multiple bone fracture [7]. The conventional treatment consists of removing the smaller bone fragments from the body in surgery, followed by the fixation of the bone using bone screws and plates [12]. In case of the removal of a larger amount of bone, the metal objects have to stay in the body, as it is too time-consuming or even not possible to regrow a large amount of bone [13].

Therefore, it would be interesting to be able to apply a material to fix multiple bone fragments during surgery, so they can be incorporated in the regrowing bone [14]. The desired material should be easily applicable during surgery, it should enable easy dispersion of dislocated bone fragments and should have fast hardening to keep the structure intact [15,16]. For these reasons, polymeric biomaterials can be a good possibility due to their ability to promote accelerated regenerative processes of tissues with slow or difficult healing. Several types and formulations have been examined for implants with adequate structural and cellular properties [17,18]. For this purpose, a UV-curing material would be interesting, as portable UV-curing devices are already applied for example in dental treatments [19]. Ideally, the material should not only be biocompatible but also enhance bone regeneration, for example by supplying necessary ceramic particles [20,21]. The material should be replaced gradually by the growing bone

in an osteotransductive manner where, it degrades under physiological conditions at a rate similar to bone formation which maintains mechanical stability of the fracture and keeps the loose bone fragments in place [22].

There are several polymers that can be easily photopolymerized using conventional initiators, such is the case of polyethylene glycol dimethacrylate (PEGDMA), which has already been reported by our group as a potential bone regeneration material [23]. However, it is possible to incorporate a temperature and/or pH sensitivity for drug delivery applications into its structure and also further enhance its potential mechanical properties [24,25]. Besides improving its mechanical properties, bio-functional monomers can also improve biocompatibility and cell proliferation, adhesion and modulate the inflammatory response of a device in a living tissue [26].

One polymer highly used as a temperature-sensitive hydrogel is Poly(*N*-isopropylacrylamide) (PNiPAAm) [27]; though, conventional PNiPAAm hydrogels from radical polymerization are fragile and weak impending their actual utilization due to their inhomogeneous network structure [28]. Consequently, researchers have been reporting that copolymerization of NiPAAm and PEGDMA can provide a temperature sensitivity to the generated structure while maintaining the favourable mechanical properties obtained for poly(PEGDMA) alone [29,30]. Even though PPEGDMA has been reported for having good biocompatibility within the human body [31], it lacks sufficient mechanical integrity to provide sufficient support for healing. For these reasons, several researchers have tried to overcome this challenge by applying different additives while obtaining an interpenetrating network, although, these materials still lacks sufficient strength comparable to the human bone [32].

In this work we developed a temperature- and pH-sensitivity hydrogel with improved strength and suitability for bone regeneration using two distinct monomer ratios for the copolymerization of NiPAAm and PEGDMA in the presence of Polyacrylic Acid (PAA). Ceramics materials were also incorporated into this monomer, nanoHaP and microsized particles of a ceramic mixture of tricalcium phosphate (TCP), Wollastonite (W) and Talc, as inorganic material to enhance bone regeneration. These ceramic particles supply the necessary building blocks for the regeneration of the inorganic bone material. Hydroxyapatite is the main ceramic present in natural bone. Consequently, both ceramics might show beneficial effects on bone healing.

2. Materials and methods

2.1 Materials

The bifunctional monomer poly(ethylene glycol) dimethacrylate (750 g/mol, PEGDMA-750), polymeric additive (polyacrylic acid, 3,000.000 g/mol, PAA), Phosphate Buffer Saline (PBS), $CaCl_2$, $(NH_4)_2HPO_4$, Minimum Essential Medium Eagle, fetal bovine serum and trypsin-ethylenediaminetetraacetic acid were obtained from Sigma Aldrich. *N*-isopropyl acrylamide (NiPAAm) was obtained from TCI chemicals. The photoinitiator used (4-(2-hydroxyethoxy)phenyl-(2-hydroxy-2-propyl)ketone, Irgacure 2959) was supplied by Ciba Specialty Chemicals. Tricalcium phosphate (TCP) supplied from Carlo Erba, Italy, Wollastonite (W) NYAD® 1250 from NYCO®, and Talc were supplied by Sigma-Aldrich, Spain. NIH 3T3 fibroblast cells were supplied by American Type Culture Collection (ATCC).

2.2 Ceramics synthesis

2.2.1 Nano hydroxyapatite

Hydroxyapatite was synthesized based on the work carried by R. Murugan *et al.* [33] *via* the wet chemical method using a slightly different concentration of 1.2 M $CaCl_2$ + 2 M $(NH_4)_2HPO_4$.

2.2.2 Ceramic synthesis of TCP, W and Talc

Ceramic grains were obtained using the procedure previously described by Canillas *et al.*[34]. Briefly, 60% TCP, 25% W, and 15% Talc (wt.%) powders were mixed by attrition milling for 1 h and dried at 60 °C which were further grounded using a tungsten mortar and sieved to a size ≤100 μm. Afterwards, the powder was compacted at 1,000 kPa/cm^2 during 60 s using uniaxial press and sintered at 1050 °C for 2 h. Grains were reground and sieved to a particle size ranging between 100 μm - 300 μm. The ceramics phases obtained on completion of the thermal treatment process were β-TCP, where Ca^{2+} is partially substituted with Mg^{2+} ($Ca_{2.81}Mg_{0.19}(PO_4)_2$), Wollastonite 2M ($CaSiO_3$) and traces of Enstatite ($Mg_2Si_2O_6$).

2.2 Syntheses

The prepolymer mixture was generated by dissolving NiPAAm in a mixture of PEGDMA and water. PAA was added slowly to the mixture as a powder under constant stirring to prevent the formation of PAA clusters within the resulting gel-like mixture. If no complete dissolution of the monomer or the polymeric additive was possible, the samples were heated to 70°C. For the samples containing ceramics, the ceramic particles were added under stirring, followed by Irgacure 2959, which was used as photoinitiator. After obtaining a homogenous prepolymer mixture, it was allowed to reach room temperature prior to UV-initiated polymerization.

For the preparation of the samples, suitable silicone moulds were chosen to generate the sample shapes necessary for testing. The prepolymer mixture was transferred to the moulds by using a spatula. The samples were cured in an UV-cube (Dr. Gröbel UV Electronics GmbH) for 10 minutes. This device is a controlled radiation source with 20 UV-tubes that provide a spectral range of between 315–400 nm at an average intensity of 10–13.5 mW/cm^2. A general reaction scheme is presented in Figure 1.
After the desired polymerization time, UV irradiation was stopped, and the samples were dried using paper tissue to remove residual monomer and moisture prior to testing. The monomers and additives applied are listed in Table 1.

Table 1. Composition (wt%) of the prepolymer mixtures polymerized under UV irradiation.

Sample	PEGDMA	NiPAAm	H_2O	Irgacure 2959	PAA	Ceramic additive
NiPAAm/PEGDMA 55:45	36.90	44.40	14.80	0.05	3.70	0.00
NiPAAm/PEGDMA 55:45+TCP	36.10	43.40	14.50	0.05	3.60	2.00 (TCP)
NiPAAm/PEGDMA 55:45+HAp	36.10	43.40	14.50	0.05	3.60	2.00 (HAP)
NiPAAm/PEGDMA 64:36	51.80	51.80	14.80	0.05	3.70	0.00
NiPAAm/PEGDMA 64:36+TCP	28.80	50.70	14.50	0.05	3.60	2.00 (TCP)
NiPAAm/PEGDMA 64:36 +HAp	28.80	50.70	14.50	0.05	3.60	2.00 (HAP)

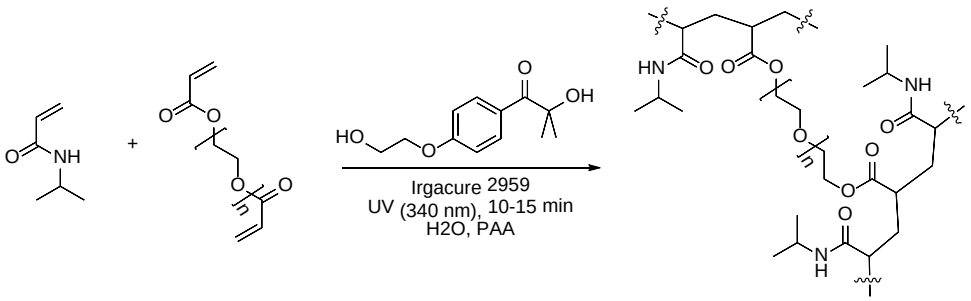

Figure 1. General reaction scheme of the UV-polymerization during the curing of the composite NiPAAm/PEDGMA.

2.3 Scanning Electron Microscope

Composite morphology was observed using a Tescan mira XMU scanning electron microscope (SEM, TESCAN, Brno, CZ) in back scattered electron (BSE) and secondary electron mode using magnifications, which ranged from 50-500x. Prior to scanning dried samples were sliced in liquid nitrogen to obtain cross-sectional regions. The samples also were gold-sputtered Baltec SCD 005 for 110 s at 0.1 mBar vacuum before testing, yielding a coating of approximately 110 nm.

2.4 Fourier transform infrared spectroscopy

Fourier transform infrared spectroscopy (FTIR) was performed on an PerkinElmer Spectrum One device and used to investigate inter- and intramolecular interactions within the investigated samples. The IR spectra were recorded in the spectral range of 4000–500 cm^{-1} and subsequent analysis was carried out using Spektragryph spectroscopy software.

2.5 Swelling studies

The dry weights of the samples (W_d) were determined after photopolymerization. Subsequently, samples were placed in distilled water to determine their water uptake (W_s). Tests were carried out in duplicate and data is presented as mean ± SD. The percentage of gel weight was calculated using following equation:

Mass increase (%) = $((W_s - W_d)/W_d)$

W_s and W_d are the weights of the hydrogels in the swollen state and the dried state, respectively.

To investigate temperature and pH responsiveness during swelling, swelling studies were carried out at 7, 20, 35, 55 and 65 °C and at pH of 2, 4, 6, 8 and 10 respectively.

2.6 Differential scanning calorimetry

For thermal analysis, differential scanning calorimetry (DSC) was carried out using DSC2920 Modulated DSC from TA instruments. All the samples were sealed in hermetic aluminium pans (Hermetic Pans, TA Instruments, USA) with the sample weight around 10-12 mg. Each sample test was performed with a heating ramp mode from 0 °C to 170 °C and heating rate of 1 °C/min under the flow of nitrogen gas.

2.7 Tensile testing

Tensile tests were performed on a Lloyd Lr10K screw-driven testing machine fitted with a 2.5 kN load cell with a bespoke 30 mm diameter testing head connected to a control computer with NeygenTM software. All samples were moulded into dumbbell shape with an average breadth of 3.5 mm and an average with of 1.5 mm in non-swollen state. The gauge length applied in the tests was 30 mm. Fixed grips were mounted onto the tensile testing machine and a crosshead speed of 50 mm/min was used. Tensile testing was performed at least in triplicate for each batch and mean stress at break, Young's modulus and strain at break values were calculated. All data and parameters calculated are presented as mean ± SD.

2.8 Cytotoxicity

2.8.1 Sample preparation

Samples were first immersed in 0.1M of sodium bicarbonate for 10 mins following immersion in ethanol for 10 mins and PBS for 10 mins prior to the elution test.

2.8.2 Cell culturing

NIH 3T3 Cells were cultured in Minimum Essential Medium Eagle (MEM) supplemented with 10% fetal bovine serum (FBS), 1% penicillin/streptomycin and 1% L-Glutamine at 37 °C with 5% CO2 in humidified incubator. The medium was changed every 2 days. Once the NIH 3T3 fibroblasts monolayer was grown to 80-90% confluence in a 75cm^2 flask, the cells were harvested by washing twice using PBS and followed by adding 5 mL trypsin-ethylenediaminetetraacetic acid (EDTA) to carry out trypsinisation and further 8ml of fresh DMEM medium was added to inactivate trypsin-EDTA solution. Finally, the

cells were centrifuged to obtain a pellet at 1500 rpm for 5 minutes, and re-suspended in the fresh MEM medium.

2.8.3 Metabolic activity (Elution test)

NIH 3T3 cells were seeded at $1x10^5$ cells per well in 96 well microtitre plates and incubated in a humidified atmosphere of 5% CO_2: 95% air at 37°C for 24 h. Cultures were exposed to pre-warmed test media containing 100 µl of 100, 75, 50, 25,0% extract samples for a further 24 h at 37 °C. 100 µL of 0.5 mg mL^{-1} MTT was added to each well and plates were incubated for a further 4 h at 37 °C. The MTT media was aspirated off and 100 µL DMSO was added to each well. Plates were shaken for 15 s and the optical densities at 540 nm was recorded. Cell viabilities were calculated using equation below: Metabolic Activity (%) = Absorbance (540 nm) treated cells / Absorbance (540 nm) untreated cells.

2.8.4 Direct contact cytotoxicity test

1 x 10^5 cells/ml cells were seeded on 6-well plate. After incubation overnight, the cells were exposed to the test samples and incubated overnight. During incubation, leachable chemicals in the test sample could diffuse into the culture medium and contact the cell layer. The morphology of the cells around the test sample was then examined and photographed using a confocal microscope connected with a digital camera. The cells are given a grade from 0 to 4 corresponding to no reactivity to severe reactivity [35]. The MTT assay was then performed to determine the cell viability.

2.8.5 Determination of p65-NF-κB by ELISA

$1x10^5$ cells/well is seeded on the 96-well plate. After incubation overnight, 100 µL of 1 mg/mL of each sample elution is added into the well and incubated overnight. The amount of NFkB p65 present in the cell lysate was then quantified using an Invitrogen™ NFkB p65 (Total) InstantOne ELISA, following the manufacturer's instruction.

2.9 Statistical Analysis.

Statistical analysis was performed with Action Stat software. A comparison between the experimental parameters within each group was performed using analysis of variance for repeated samples, followed by the nonparametric Friedman test. For comparison between

groups, at each experimental moment the parametric Student's *t* test was used for independent samples. Both tests were applied at the 5% level of significance.

3. Results and Discussion

Even though the photopolymerization of the chosen monomers occurred at a very fast rate and within minutes, it was still necessary that the uncured resin had a sufficient viscosity to enable easy retention of multiple bone fragments as intended in the final application. The prepolymer mixture function as a cream-like texture that can be applied easily with a medical tool or a simple spatula. Therefore, high molecular weight PAA (3.000.000 g/mol) was used as additive to improve applicability of the prepolymer mixture for example in surgeries, helping it acting as cement and as implant [36,37]. The studied polymers in this work polymerized evenly without phase separation. The possible photopolymerization scheme of this material is shown in Figure 2.

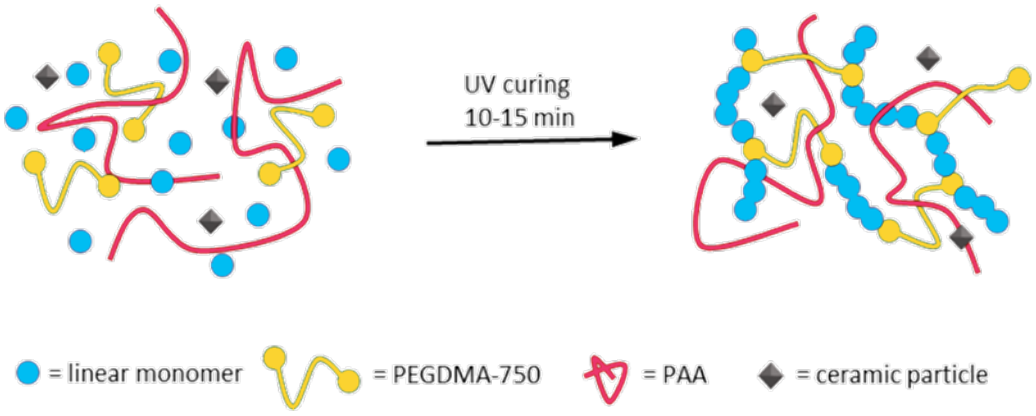

Figure 2. UV-curing reaction of a prepolymer mixture containing the necessary monomeric structures as well as additives suitable during application.

3.1 Morphology analysis

To analyse the effect of ceramic addition on the morphology of the hydrogel, SEM images of the cross-section of the materials with or without ceramics were investigated in the samples of NiPAAm/PEGDMA 64:36 (Figure 3); it is possible to observe that the ceramics were embedded in the hydrogel. Furthermore, TCP and nano-HAp presented no signs of agglomeration that could lead to a poor intimate contact between the ceramic and the polymeric material. The additives were well dispersed and different sizes of the ceramic particles can be observed (Figure 3b). However, in the case of nano-HAp (Figure

3c) it is possible to observe the small nanoparticles of HAp also incorporated into the structure of this polymeric material.

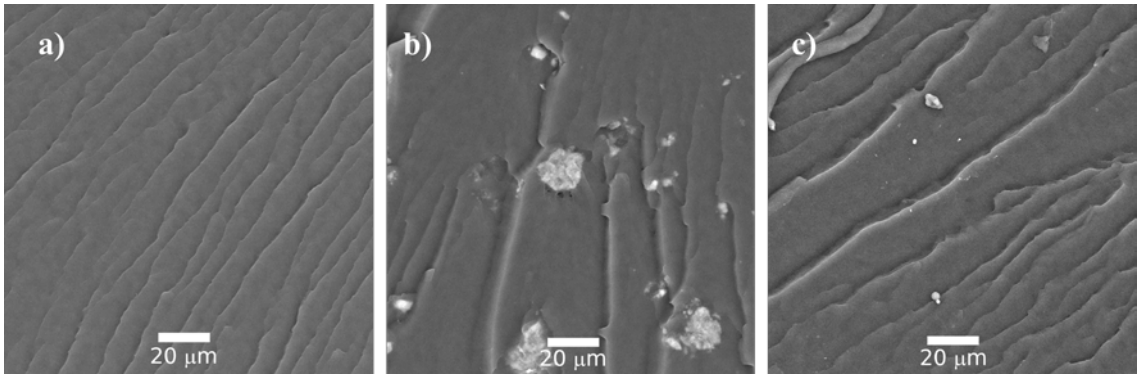

Figure 3. Scanning electron microscope images of the cross-section of pure (a) NiPAAm/PEGDMA 64:36; (b) NiPAAm/PEGDMA 64:36+TCP and (c) NiPAAm/PEGDMA 64:36+HAp.

3.2 FTIR Measurements

3.2.1 Effect of monomer addition

To gain a wider knowledge about interactions in the composites, FTIR measurements were carried out. The expected signals for NiPAAm and PEGDMA units can be found in the spectra (Figure 4-5) – guided lines were drawn to these figures to simplify the analysis. The reaction of the acrylate double bonds in photopolymerization decreases the intensity of the PEGDMA signals at 815 cm^{-1} (twisting vibration of the acrylic CH_2=CH bond), at 1410 cm^{-1} (deformation of CH_2=CH bond) and at 1167 cm^{-1} (acrylic C=O bond) [38,39]; for NiPAAm the peaks of C=C and CH_2=C stretching at 1620, 1409, 986, 917, 808 and 708 cm^{-1} [40,41] disappeared, confirming the consumption of this monomer in photopolymerization. The assignment of the FTIR signals to PEGDMA and NiPAAm units within the copolymer is in agreement with other reports in literature [42–44].

Nevertheless, the investigated material in this work also contained polyacrylic acid in its structure to provide support and generate an interpenetrating network structure [45,46] that could reinforce the material. For these reasons, the spectrum of pure PAA is also included in Figure 4.

The spectra of the studied samples contains the pattern of the PAA as well as it is detailed in the regions i, ii, and iii of Figure 4. The sharpest and strongest band is found at 1702 cm^{-1} (C=O carbonyl stretching vibration in Figure 4 region i). When incorporated into the

PEGDMA/NiPAAm hydrogel, this peak disappears but a new peak at 1642 cm^{-1} is formed. This could represent an interaction with the NiPAAm units (signal at 1656 cm^{-1}, C=O stretching of amide bond [47] and the PEGDMA monomer (signal at 1637 cm^{-1}, C=C stretch vibration of the methacrylate [23]) present in the hydrogel. These interactions can occur at the expense of cyclic dimers of PAA [48].

This effect can also be observed in two other regions of the PAA band; the first is at 800 cm^{-1} (CH_2 twisting and stretching of the PAA backbone, region ii of Figure 4), where it overlaps with the double bond region of NiPAAm at 808 cm^{-1} and a signal of low intensity of PEGDMA at 815 cm^{-1}. The second region is at the large broad signal between 1132 cm^{-1} and 1320 cm^{-1} of PAA which appears to be incorporated into the NiPAAm/PEGDMa polymer produced, although as a shortened profile which is unique as it is not perceived in the NiPAAm and PEGDMA spectra alone. Nonetheless, the signal maxima of PAA within this region at 1241 cm^{-1} and 1170 cm^{-1} (CH_2 and CH-CO vibrations, respectively) are within the region of a very defined NiPAAm band at 1244 cm^{-1}, (isopropyl groups, [49]) and a small band of PEGDMA at 1250 cm^{-1}, which could justify the signal shift towards to 1247 cm^{-1} in the studied spectra. Furthermore, the defined signal of NiPAAm in this region is shortened in the studied material; therefore, the shortening of the signals in this region also confirms successful incorporation of these three components into the overall structure.

Lastly it is the broad signal of –OH group presented for PAA (2700–3700 cm^{-1}) (intermolecular cyclic dimer interaction from the –COOH group), in which the group –NH stretching band of NiPAAm at 3282 cm^{-1} has weakened and broadened and tends to overlap with the broad band of carboxylic group (–COOH) of PAA in 2400–3500 cm^{-1} [48].

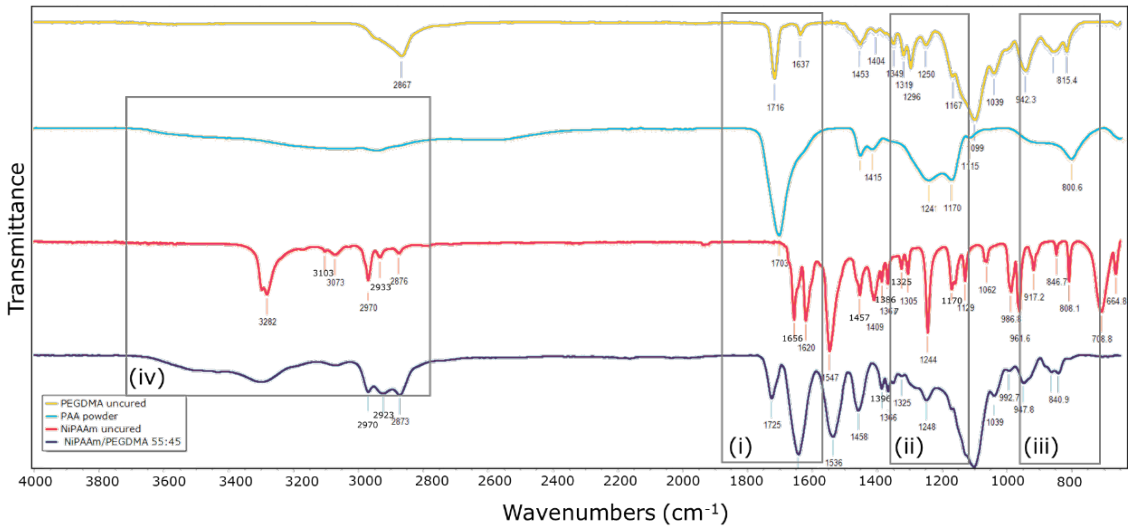

Figure 4. FTIR of the monomers and polymers used before and after polymerization of the hydrogel.

3.2.2 Effect of varying monomer content

The effect of varying the PEGDMA/NiPAAm monomer ratio in the studied materials can be determined by two major bands at 1716 cm^{-1} and 1099 cm^{-1} (guided lines (i) and (ii) in Fig 5.a). The signal at 1716 cm^{-1}, which corresponds to the C=O stretching obtained in pure PEGDMA spectra (from Fig. 4), the peak intensity increases with increasing PEGDMA content. Also, the broad signal of pure PEGDMA at 1099 cm^{-1} (area of carbonyl groups from Fig. 4) is well perceived in the samples investigated in this work. Additionally, a shift towards the signal position of the PEGDMA monomer occurs with increasing PEGDMA content. The effect of NiPAAm in the studied samples also follows a similar pattern, the signal at 1547 cm^{-1} (N-H stretching of amide II, guided line iii) shifted towards lower wavenumbers and shortened with increasing content of PEGDMA monomer. Although, there is a variation on peak intensity when varying the monomer ratio following the same profile. No new peaks are visible when increasing the amount of these monomers.

3.2.3 Effect of ceramic addition

Finally, we investigate the effect of the addition of ceramics to the studied material, from Figure 5b-c. It is possible to see that TCP shows characteristic absorption bands in the range between 800 and 1200 cm^{-1}. The signals at 682 and 902 cm^{-1} are assigned to the SiO_2 groups of wollastonite [50]. The signals at 938, 968, 1022 and 1107 cm^{-1} are

attributed to PO_4^{3-} groups from TCP [51]. In the case of nano-HAp the peak at 1023 cm^{-1} ($PO_4^{3-}{}_{V3}$ stretching) and 962 cm^{-1} ($PO_4^{3-}{}_{V1}$ stretching) [52].

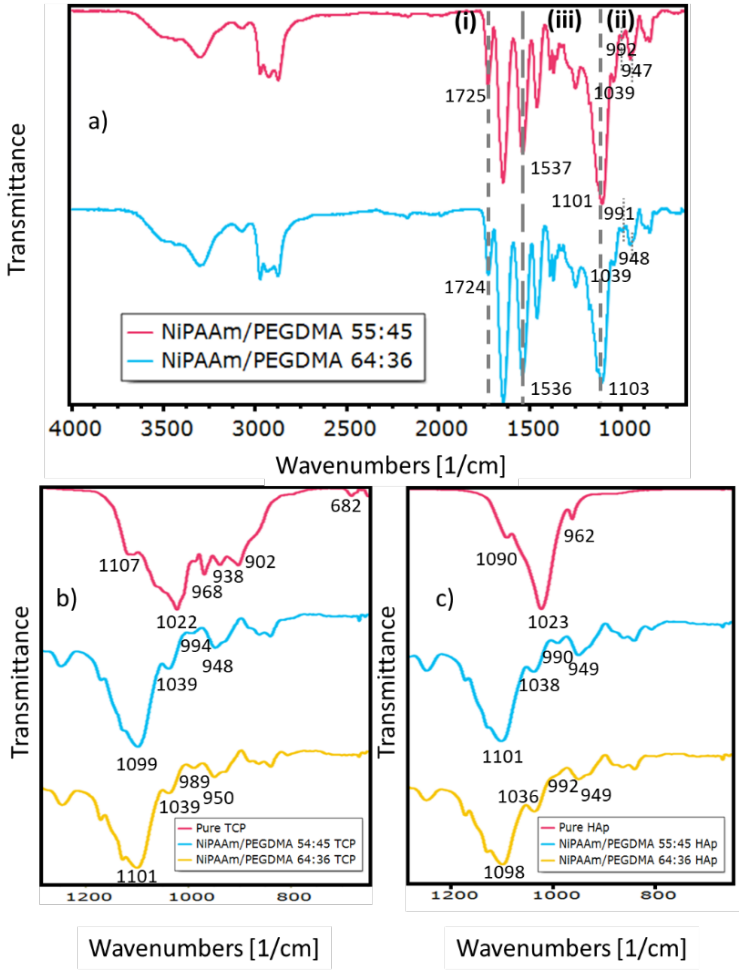

Figure 5. FTIR of the studied hydrogels (a) without ceramics and with (b) TCP and (c) HAp – the spectra of the ceramics are also included.

Interactions with the ceramics were not visible clearly, as their amount in the composites is relatively low and stronger signals corresponding to the polymers were found in the important regions. However, earlier reports of our group suggest that the synthesis and interactions of these ceramics can be analysed by the absence of signals caused by calcium carbonate groups between 1400 and 1500 cm^{-1} [53]. Regions of the polymer within the area of the main signals of the additives ceramics appear to shift the bands of the polymers in the hydrogel towards the ones of the main signals of ceramics. The structure-interaction of the ceramic and the monomers after photopolymerization discussed herein is represented in Figure 2.

3.2 Swelling Studies

Swelling studies (Figure 6) show the swelling ratio of all samples investigated. As swelling of the samples is dependent on the temperature, the swelling behaviour was investigated at different temperatures. It can be seen that the swelling ratio is very low and although a temperature sensitivity does occur within these samples, the lower critical solution temperature (LCST) is not within the studied temperature of this material. Nonetheless, PNiPAAm shows a transition from hydrophilic to hydrophobic behaviour around 37°C, which might result in increased hydrophobicity of the material when incorporated in the body [43]. For the samples studied in this work, we deduce from the results obtained in the swelling studies that the LCST could lies at a temperature below 7°C. Nevertheless, there are reports of PEGDMA/NiPAAm copolymers with a LCST similar to pure PNiPAAm; they present swelling ratios twenty times higher than the ones reported in this work [29] and at much lower content of PEGDMA[30].

Nonetheless, samples swollen at 37 °C presented a 70% mass increase. For a material used as implant, swelling is a required feature to some extent as it eliminates dead space where bacteria can colonize, however it should be controlled to prevent limb swelling which could cause patient pain. The values obtained from swelling are lower than of the ones reported for PEGDMA and NiPAAm homopolymers [23]. We deduce that the PAA acting as an interpenetrating network may influence temperature sensitivity by reinforcing the structure, resulting in a low swelling ratio and lowered LCST. However, there was no significant difference between the hydrogels containing ceramic additives and the hydrogels without ceramics for temperatures higher than 37°C. For lower temperatures, ceramic addition slightly increases the swelling ratio. Although, it is possible that ceramics increase the swelling properties while also increasing its mechanical properties [34].

These samples also presented a pH sensitivity. A statistically significant difference from basic to acidic environment in swelling was found for all of the samples. Although, in between the groups, hydrogels containing HAp exhibited significantly lower values than hydrogels without ceramics.

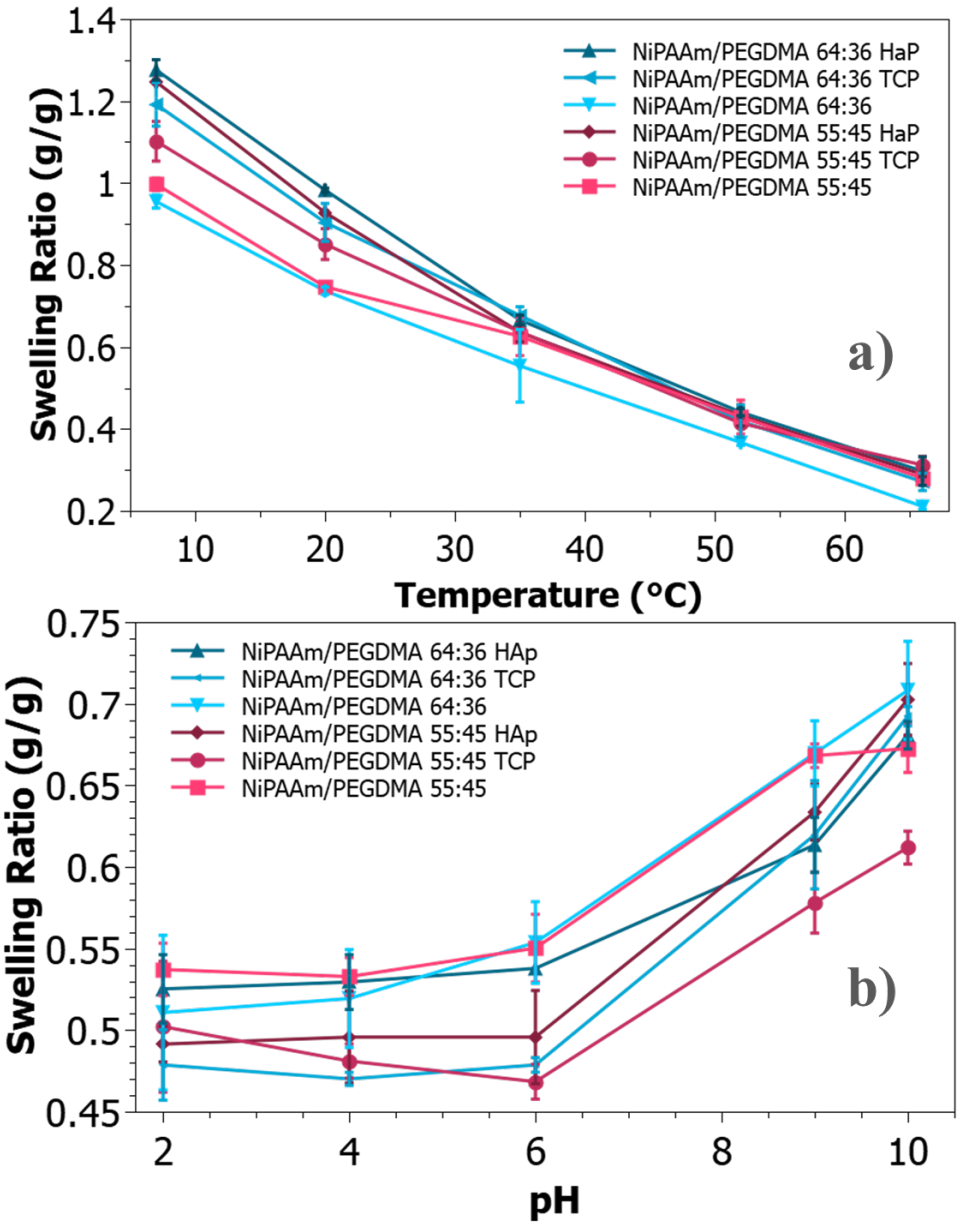

Figure 6. Swelling ratio of the studied materials at different temperatures and pH values reveals double simuli responsiveness of the hydrogel.

3.3 Mechanical properties

As it can be seen from Figure 7, adding a suitable polymer can increase mechanical properties of a composite. Standard values of NiPAAm and PEGDMA photopolymers are reported on the order of 10-80 kPa and 5-10 MPa respectively [23,32,54], and there have been several efforts to improve the mechanical properties of PNiPAAm without losing the temperature responsiveness of these materials [32].

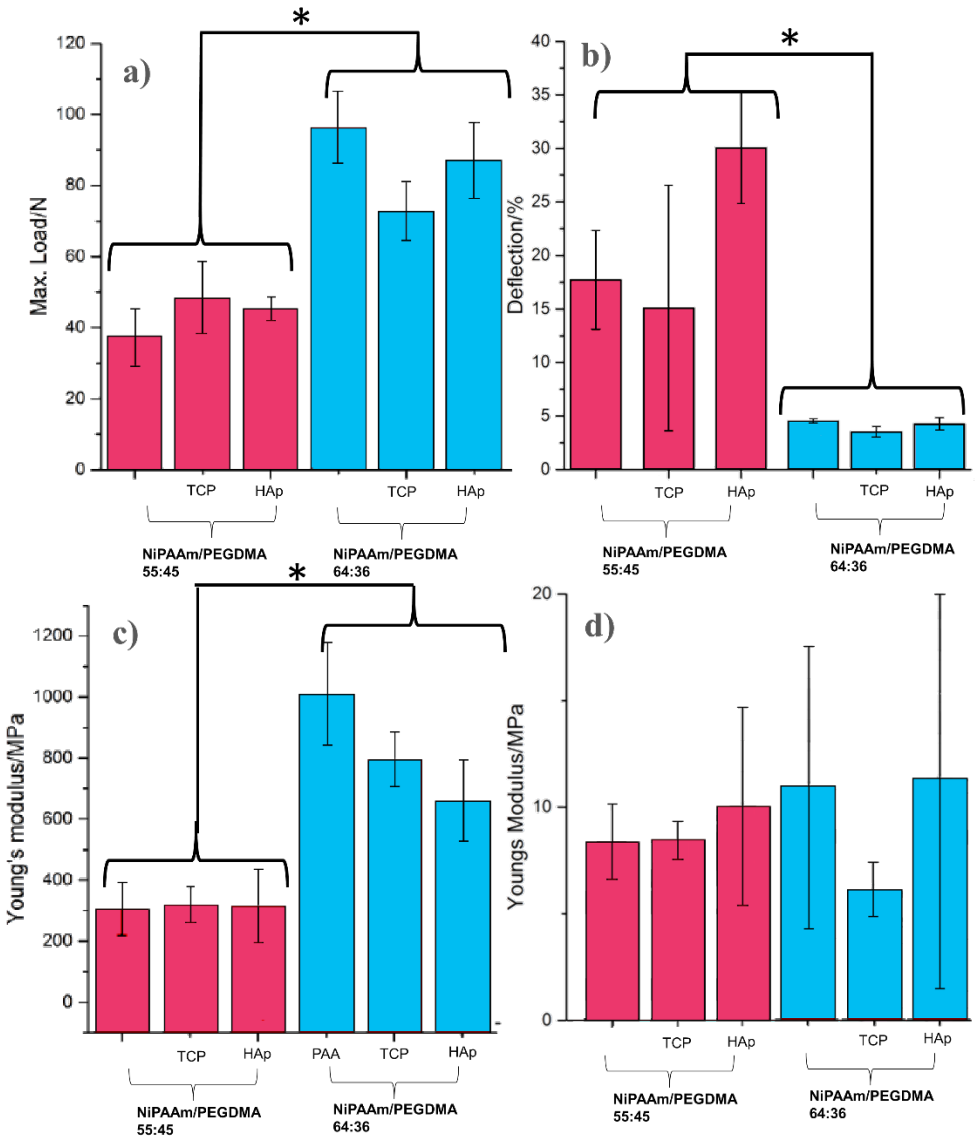

Figure 7. Results of a) maximum load, b) Deflection at break and Young`s modulus calculated from tensile tests in dry c) and swollen d) samples. (*) corresponds to statistically significant difference between groups ($p \leq 0.05$).

Tensile tests obtained in this work show higher values in dried state: ~300 MPa and ~1000MPa, depending on the monomer ratio (Figure 7c). Also, tensile tests on swollen samples also show values much higher than the ones reported for PNiPAAm (~10KPa, [32]). Although these are very interesting mechanical properties, the materials exhibit a low swelling capacity and LCST. Nonetheless, considering this as an implant material, these are interesting results and, we believe, that the high molecular weight PAA does not only increase the viscosity of the prepolymer mixture assuring a better applicability for the multiple bone fraction application as intended, but it also strengthens the composite,

possibly by formation of strong hydrogen bonds. With PAA, interactions between the carbonyl group between the monomers and the hydrogen atoms in acrylic acid moieties are possible. Figure 7 shows further that increasing the amount of linear monomer in case of the NiPAAm-containing composites increases mechanical properties. Apparently, NiPAAm is able to form strong interactions which are disturbed if overly high amounts of PEGDMA or ceramics are applied.

On the other hand, polymers containing larger amounts of NiPAAm were also less deflectable (Figure 7b). Even if a certain degree of flexibility might be beneficial for the material in order to generate space for the regenerating bone, a low deflection to break combined with a high mechanical strength would mimic properties of natural bone. In any case, the maximum deflection of bone before break is significantly lower as for the polymers investigated here.

The use of ceramics for improvement of biocompatibility has been reported by several authors [51]. However, depending on the amount of ceramic content, its mechanical properties could be significantly varied. Therefore, the amount of ceramic used in this work around 3wt% was not only beneficial to improve the biocompatibility but is also able to maintain the integrity of the pure PAA/P(NiPAAm-*co*-PEGDMA) material. However, it is also worth to note that the maximum amount of nano-HAp that can be suspended in the prepolymer mixture without precipitation is quite low, around maximum 7 wt% [55].

Further, it can be seen that the addition of ceramic additives decreases the mechanical properties for higher amounts of NiPAAm in the copolymer. This was not the case for lower amounts of NiPAAm in the copolymer (not statistically significant). Nonetheless, the decrease of the values of Young's modulus are not drastically when samples are swollen. The Young's modulus for all samples tested is in the range of 5-10 MPa.

Nevertheless, the comparison of the composites with the mechanical properties of human bone show that the appliance of the UV curing materials without the support of conventional screw plates used for bone fixation is not possible at the moment. This can also be further associated with the maximum load on tensile tests results for these polymers, resulting in values of 80 N and 40 N depending on the ratio of the monomers. Although these should be accompanied by its ultimate tensile strength, it can already give an indication that these materials still require further improvement if used exclusively.

Therefore, although this material can contribute to load bearing, it probably will need to be used in conjunction with a fixation plate to take most of the load. It is important to note that even though the young's modulus values of the materials cannot reach values comparable to mammalian bone, it is still higher than what is currently possible to achieve with conventional NiPAAm monomers and conjugates [32].

3.4 Glass transition temperature (T_g)

The influence of the monomer ratio, nano-HAp and TCP on the glass transition temperature of the P(NiPAAm-*co*-PEGDMA) composites was analysed *via* DSC (Figure 8).

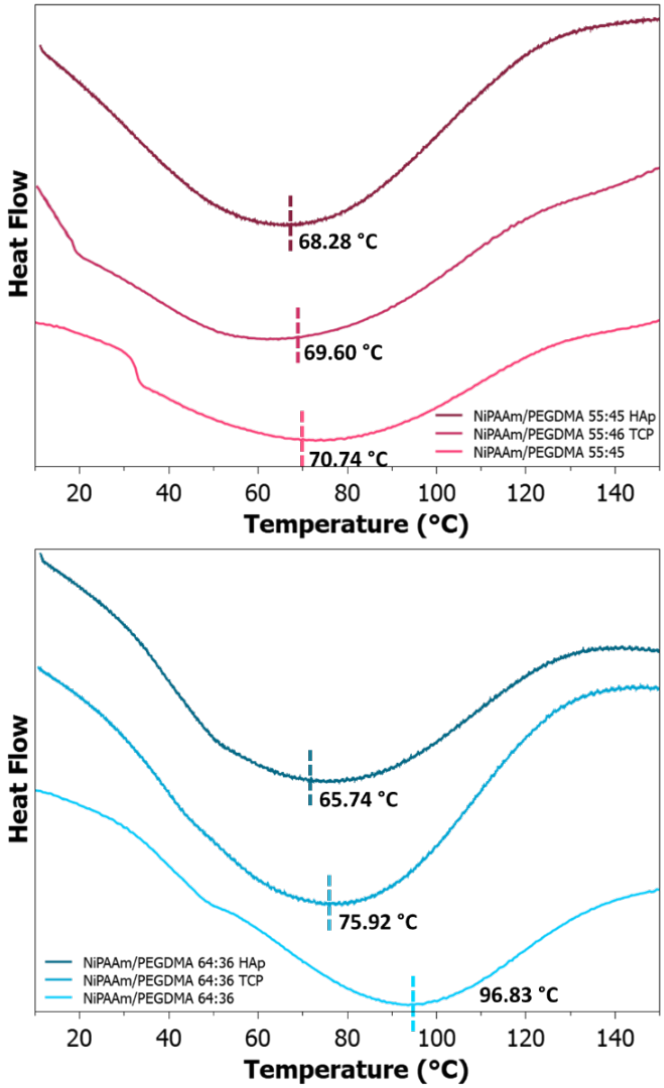

Figure 8. DSC to investigate the T_g of the studied hydrogels. It is possible to observe that ceramic additives as well as an increased amount of PEGDMA – leads to a decrease of the T_g.

The values of T_g, for samples without ceramic, show that a higher amount of NiPAAm in the copolymer led to an increase in its T_g – which is in agreement with mechanical properties results; the effect of adding a comonomer such as PEGDMA, which has flexible segments, leads to a more flexible polymer and is coherent with the results obtained from deflection at break in the mechanical testing. Similar behaviour has already been reported [30].

When ceramics are introduced into this polymer, its T_g values are further reduced; it has been reported that ceramic additives in a polymer composite can act as a plasticizer by inhibiting a degree of intermolecular bonding in the polymer matrix [34]. The T_g values are only slightly reduced when there is a higher quantity of PEGDMA; when reducing the amount of this monomer and increasing NiPAAm content, an even further reduction of the T_g values can be observed, which is in agreement with what was obtained from tensile results. Comparing the different ceramic particles, it can be seen that adding HAp to this hydrogel structure gives the lowest T_g values.

3.5 Cytotoxicity

To investigate potential toxicity of the studied materials on cells, cytotoxicity tests were carried out using fibroblasts NIH 3T3. The results exhibit that cell metabolic activity for all samples are all larger than 70% (shown in Figure 9) and that the investigated materials can be considered as non-toxic. It is possible to observe that there is a significant difference in toxicity depending on the amount of PEGDMA monomer. With higher amounts, the polymer stands with a mean of viability of 70.94% almost at the threshold to be considered non-toxic. When decreasing the amount of this monomer, the cellular viability is significantly higher. Reports on PEGDMA using Irgacure 2959 as initiator has shown that it is non-toxic for mESC and hNSC cells [31].

Contrarily, reports on toxicity of the monomers acrylic acid and methacrylic acid suggest that both have ability to inhibit the growth of fibroblasts [56]. Therefore, it is possible that PAA functionalities, depending on their incorporation and interactions within the material, cause cytotoxicity in these studies.

Nonetheless, the addition of ceramics to the materials containing higher quantity of PEGDMA exhibit a significant improvement of cellular viability, with HAp having a larger effect than TCP. However, in the case of the hydrogel containing lower amounts of PEGDMA no significant differences were perceived with the addition of the ceramics.

We deduce that this factor could be due to the link to the phosphate groups that might be formed here.

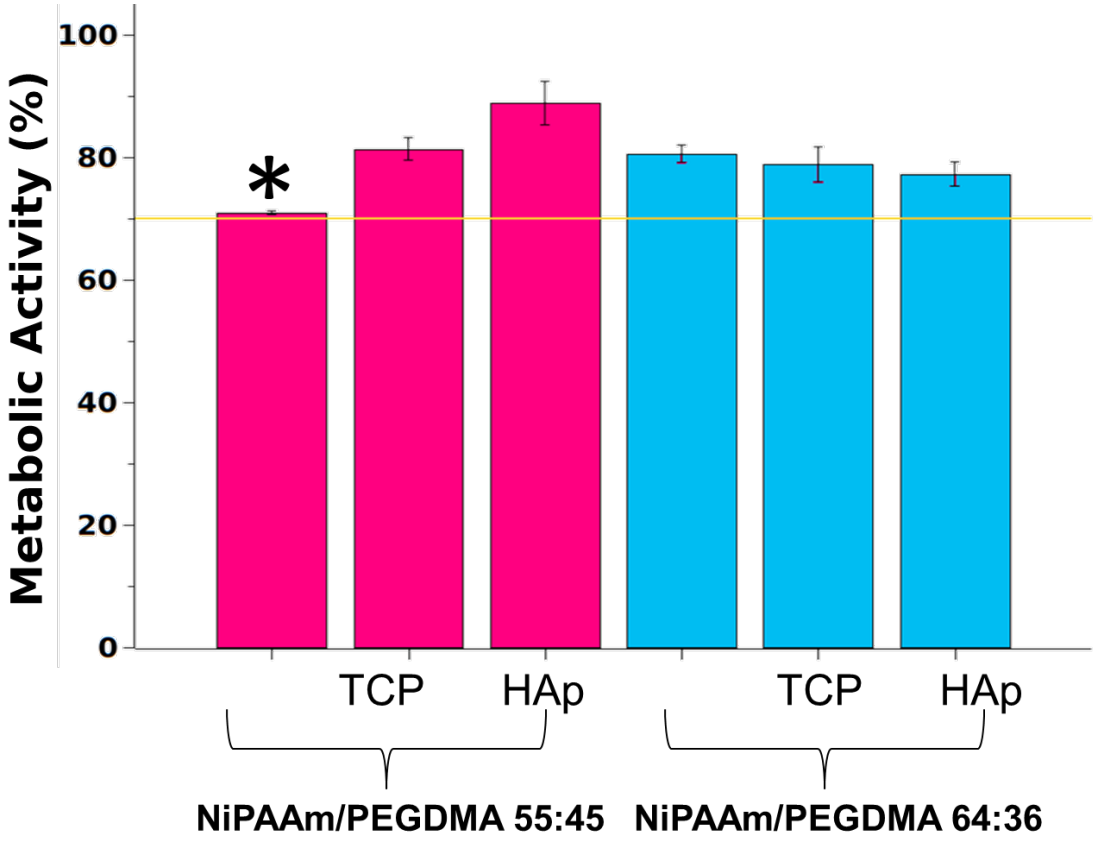

Figure 9. Cellular metabolic activity using NIH 3T3 cells of the studied hydrogels. (*) corresponds to statistically significant difference between samples ($p \leq 0.05$).

Cell morphology and cell viability MTT assays were performed for all samples (Figure 10). Herein, hydrogels containing TCP were given a grade of 1, meaning both samples have a slight reactivity upon the cell layers, but can be considered non-cytotoxic. The cells remained attached to the well and only some rounded cells are observed, indicating they are alive and are not suffering from a toxic response. In addition, both samples have cell viability of 72%. Conversely, all other samples have cell viability below 70%. Half or more than half of the cells stop growing and are rounded or detached from the well, indicating they either dead or dying. Hence, these samples are categorised into Grade 3 which they have moderate reactivity to cells and considered cytotoxic according to the procedure adopted [35].

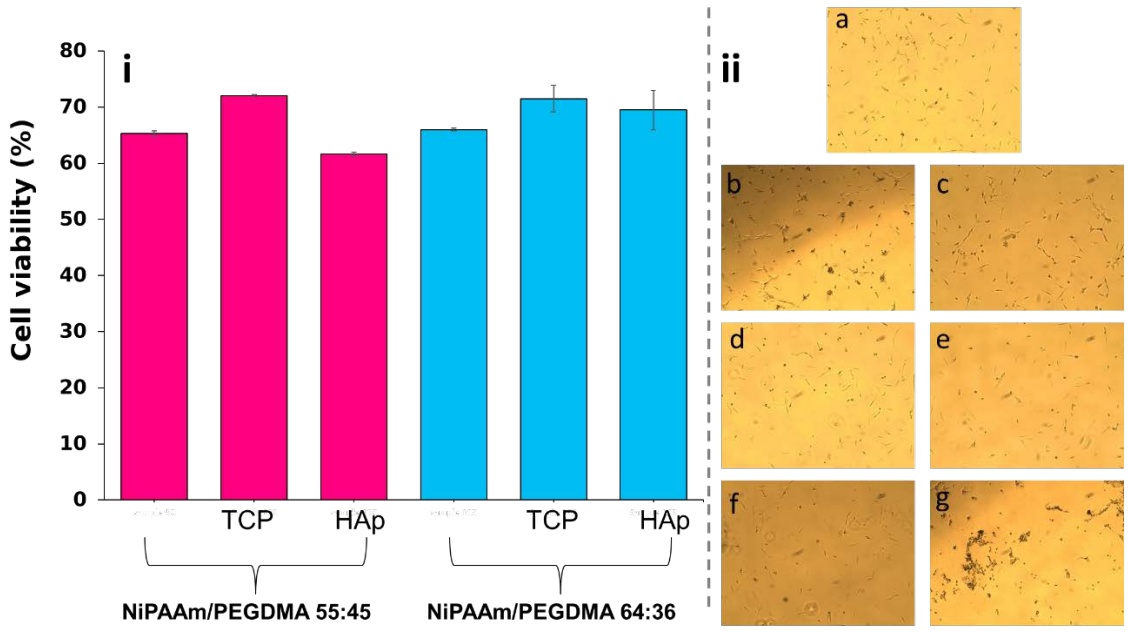

Figure 10. Cytotoxicity tests to evaluate cell activity where i) Direct contact cytotoxicity test and ii) morphology of the cells after directly incubated with the hydrogels – a) control; b) NiPAAm/PEGDMA 55:45 with c) TCP and d) HAp, e) NiPAAm/PEGDMA 64:36 with f) TCP and g) HAp

A study on the Nuclear Factor kappa B (NF-κB) p65 signalling were investigated using InstantOne ELISA kit (Figure 11). The 3T3 cells were incubated in contact with the studied hydrogels to stimulate the signalling pathway. The total NF-κB p65 protein is then determined from the cell lysate using the NF-κB (Total) antibody cocktail. It is noted that the NF-κB p65 (Total) antibody recognizes NF-κB p65 irrespective of phosphorylated NF-κB p65. NF-κB is a transcription factor related to an inflammatory process and is strongly implicated in initiation of pro-inflammatory target gene expression, e.g., IL-6, IL-8 or COX-2 [57]. Nonetheless, studies have shown that NF-κB plays a crucial and reciprocal role in fibroblast healing because it monitors the expression of genes involved in inflammatory and oxidative stress response by inducing protein expression levels of IKKα, IKKβ, p65 and also the differentiation, proliferation, apoptosis and cell adhesion [58]. Furthermore, recent studies indicate that it plays a key role in the regeneration for various biomaterials [59,60].

Correlating these data with the cell adhesion tests it could be deduced that the NF-κB also plays an important role in the proliferation and cell adhesion of the investigated hydrogels by the increased reporter activity of NF-κB in a dose-dependent manner (Fig. 11).

Increased activity was associated with an increased nuclear translocation of p65, a major subunit of NF-κB. The ceramics added in the structure of the hydrogels exhibited significant influence, and cells in contact with TCP-containing samples showed the highest cellular viability on direct contact assay and the highest activation of the nuclear factor κB, which is in agree with our hypothesis. However, the samples containing HAP exhibited a significant decrease of cell viability with a decrease on PEGDMA monomer, this trend follows the cellular metabolic activity (Fig. 9). These might be due to the slightly different concentration used to produce the nano-HAp – leading to a slightly different ratio of Ca/P formed.

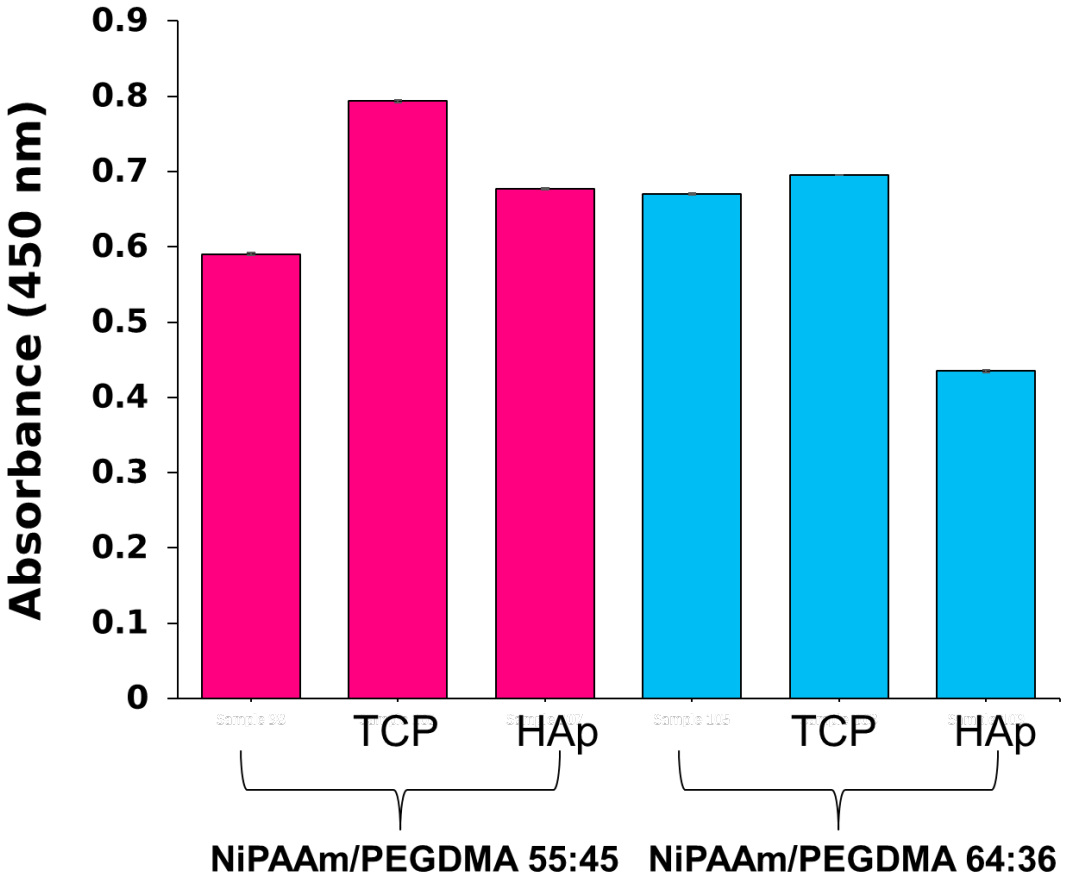

Figure 11. Phosphorylated NF-κB activity for the studied hydrogels. It is possible to observe an increase in cell viability for samples containing TCP ceramics.

Nonetheless, to obtain these results some primary steps were necessary in order to remove any unreacted monomer and neutralize the acrylic acid. In the case of application of this polymer, it would be standard in surgery to flush the wound with saline to remove any debris. So, either a neutralization washing with a weak base such as sodium carbonate or

washing with copious amounts of saline prior to closure of the wound, which is routinely done to clean the surgical area, would be necessary.

Conclusion

In this work, IPN hydrogels composed of NiPAAm and PEGDMA as UV-curable monomers, coupled with PAA as polymeric additive with varying concentrations of monomers and ceramic additives, were investigated as an alternative to mechanical fixation of bone fragments in multiple bone fracture surgeries. These materials presented an IPN structure confirmed by FTIR. This structure led to remarkable values of mechanical properties. Although these were reduced when swollen, they are higher than what is currently found in literature. Furthermore, these hydrogels presented low values of swelling. Still, they presented a temperature-response with an LCST below 7°C as well as pH-responsiveness and they presented variations on the toxicity, whereas the addition of TCP in the structure of these hydrogels presented to be non-toxic for the cells investigated (fibroblasts). On the other hand, ceramics added to the structure varied the values of mechanical properties depending on the NiPAAm/PEGDMA monomer ratio. Finally, the values of T_g of the composites were also shown to be dependent on monomer ratio and ceramic content. Overall, these initial results support the hypothesis that a tailorable in situ UV curable resin could potentially be used to consolidate bone fragments for direct repair of multiple fractures.

Acknowledgements

This study was financed in part by the Coordenação de Aperfeiçoamento de Pessoal de Nível Superior - Brasil (CAPES) - Finance Code 001 and Science Without Borders. We also thank Maria Canillas for supplying the TCP ceramic materials.

References

[1] Tavassoli H, Alhosseini S N, Tay A, Chan P P Y, Weng Oh S K and Warkiani M E 2018 Large-scale production of stem cells utilizing microcarriers: A biomaterials engineering perspective from academic research to commercialized products *Biomaterials* **181** 333–46

[2] Harris J J, Lu S and Gabriele P 2018 Commercial challenges in developing biomaterials for medical device development *Polym. Int.* **67** 969–74

[3] Changi K, Bosnjak B, Gonzalez-Obeso C, Kluger R, Rodríguez-Cabello J C,

Hoffmann O and Epstein M M 2018 Biocompatibility and immunogenicity of elastin-like recombinamer biomaterials in mouse models *J. Biomed. Mater. Res. Part A* **106** 924–34

[4] Raita Y, Komatsu K and Hayakawa T 2015 Pilot study of gingival connective tissue responses to 3-dimensional collagen nanofiber-coated dental implants *Dent. Mater. J.* **34** 847–54

[5] Agarwal R, González-García C, Torstrick B, Guldberg R E, Salmerón-Sánchez M and García A J 2015 Simple coating with fibronectin fragment enhances stainless steel screw osseointegration in healthy and osteoporotic rats *Biomaterials* **63** 137–45

[6] Devine D, Leitner M, Perren S, Boure L and Pearce S 2009 Tissue reaction to implants of different metals: A study using guide wires in cannulated screws *Eur. Cells Mater.* **18** 40–8

[7] Park Y S and Kim H S 2014 Prevention and treatment of multiple osteoporotic compression fracture *Asian Spine J.* **8** 382–90

[8] Chattopadhyay S and Tripathi C 2010 Skull fracture and haemorrhage pattern among fatal and nonfatal head injury assault victims - a critical analysis. *J. Inj. Violence Res.* **2** 99–103

[9] Karatzas A D, Paridis D, Kozyrakis D, Tzortzis V, Samarinas M, Dailiana Z and Karachalios T 2017 Fanconi syndrome in the adulthood. The role of early diagnosis and treatment *J. Musculoskelet. Neuronal Interact.* **17** 303–6

[10] Bhan A, Rao A D and Rao D S 2010 Osteomalacia as a result of vitamin D deficiency *Endocrinol. Metab. Clin.* **39** 321–31

[11] Pearce S H S and Cheetham T D 2010 Diagnosis and management of vitamin D deficiency *Bmj* **340** b5664

[12] Zhang W, Zheng Z, JI Y and Qiao Z 2008 Classification to guide internal fixation for tibial fracture *Chinese J. Traumatol. (English Ed.* **11** 375–9

[13] Postacchini F and Cinotti G 1992 Bone regrowth after surgical decompression for lumbar spinal stenosis *J. Bone Joint Surg. Br.* **74** 862–9

[14] Fini M, Giavaresi G, Aldini N N, Torricelli P, Botter R, Beruto D and Giardino R 2002 A bone substitute composed of polymethylmethacrylate and α-tricalcium phosphate: results in terms of osteoblast function and bone tissue formation *Biomaterials* **23** 4523–31

[15] Kohli N, Ho S, Brown S J, Sawadkar P, Sharma V, Snow M and García-Gareta E 2018 Bone remodelling in vitro: Where are we headed?:-A review on the current understanding of physiological bone remodelling and inflammation and the strategies for testing biomaterials in vitro *Bone* **110** 38–46

[16] Sheikh Z, Hasanpour S and Glogauer M 2018 Bone Grafting *Mandibular Implant Prostheses* (Springer) pp 155–74

[17] Miculescu F, Maidaniuc A, Voicu S I, Thakur V K, Stan G E and Ciocan L T 2017 Progress in Hydroxyapatite–Starch Based Sustainable Biomaterials for Biomedical Bone Substitution Applications *ACS Sustain. Chem. Eng.* **5** 8491–512

[18] Pandele A M, Comanici F E, Carp C A, Miculescu F, Voicu S I, Thakur V K and Serban B C 2017 Synthesis and characterization of cellulose acetate-hydroxyapatite micro and nano composites membranes for water purification and biomedical applications *Vacuum* **146** 599–605

[19] Santini A, Gallegos I T and Felix C M 2013 Photoinitiators in dentistry: a review *Prim. Dent. J.* **2** 30–3

[20] de Lima G G, Lyons S, Devine D M and Nugent M J D 2018 Electrospinning of Hydrogels for Biomedical Applications - Hydrogels: Recent Advances ed V K Thakur and M K Thakur (Singapore: Springer Singapore) pp 219–58

[21] Ramesh N, Moratti S C and Dias G J 2018 Hydroxyapatite–polymer biocomposites for bone regeneration: A review of current trends *J. Biomed. Mater. Res. Part B Appl. Biomater.* **106** 2046–57

[22] Goetten de Lima G, Halligan S, Geever L, Dalton M, McConville C and Nugent M J D 2019 3. Controlled release of poorly soluble active ingredients from bioresorbable polymers *Bioresorbable Polymers* ed D Devine (Berlin, Boston: De Gruyter) pp 47–68

[23] Killion J A, Geever L M, Devine D M, Kennedy J E and Higginbotham C L 2011 Mechanical properties and thermal behaviour of PEGDMA hydrogels for potential bone regeneration application *J. Mech. Behav. Biomed. Mater.* **4** 1219–27

[24] Yuan H, Li B, Liang K, Lou X and Zhang Y 2014 Regulating drug release from pH-and temperature-responsive electrospun CTS-g-PNIPAAm/poly (ethylene oxide) hydrogel nanofibers *Biomed. Mater.* **9** 55001

[25] Zhang D, Tan Q, Luo J and Lv Q 2018 Evaluating the angiogenic potential of a novel temperature-sensitive gel scaffold derived from porcine skeletal muscle tissue *Biomed. Mater.* **13** 55003

[26] Wróblewska-Krepsztul J, Rydzkowski T, Michalska-Pożoga I and Thakur V K 2019 Biopolymers for Biomedical and Pharmaceutical Applications: Recent Advances and Overview of Alginate Electrospinning *Nanomaterials* **9** 404

[27] Zhang N, Shen Y, Li X, Cai S and Liu M 2012 Synthesis and characterization of thermo-and pH-sensitive poly (vinyl alcohol)/poly (N, N-diethylacrylamide-co-itaconic acid) semi-IPN hydrogels *Biomed. Mater.* **7** 35014

[28] Takigawa T, Yamawaki T, Takahashi K and Masuda T 1998 Change in Young's modulus of poly (N-isopropylacrylamide) gels by volume phase transition *Polym. Gels Networks* **5** 585–9

[29] Son K H and Lee J W 2016 Synthesis and characterization of poly(ethylene glycol) based thermo-responsive hydrogels for cell sheet engineering *Materials (Basel).* **9**

[30] Li B, Zhong Q, Li D, Xu K, Zhang L and Wang J 2018 Influence of Ethylene Glycol Methacrylate to the Hydration and Transition Behaviors of Thermo-Responsive Interpenetrating Polymeric Network Hydrogels *Polymers (Basel).* **10** 128

[31] Wilems T S, Lu X, Kurosu Y E, Khan Z, Lim H J and Smith Callahan L A 2017 Effects of free radical initiators on polyethylene glycol dimethacrylate hydrogel properties and biocompatibility *J. Biomed. Mater. Res. - Part A* **105** 3059–68

[32] Abdul M, Su Y and Wang D 2018 Mechanical properties of PNIPAM based

hydrogels : A review Mechanical properties of PNIPAM based hydrogels : A review *Mater. Sci. Eng. C* **70** 842–55

[33] Murugan R and Ramakrishna S 2004 Bioresorbable composite bone paste using polysaccharide based nano hydroxyapatite *Biomaterials* **25** 3829–35

[34] Canillas M, De Lima G G, Rodríguez M A, Nugent M J D and Devine D M 2016 Bioactive composites fabricated by freezing-thawing method for bone regeneration applications *J. Polym. Sci. Part B Polym. Phys.* **54** 761–73

[35] Vidal M N P and Granjeiro J M 2017 Cytotoxicity Tests for Evaluating Medical Devices: An Alert for the Development of Biotechnology Health Products *J. Biomed. Sci. Eng.* **10** 431–43

[36] Smith D C 1972 Surgical cements from zinc oxide and aqueous poly (acrylic acid)

[37] Wallace M L, Ellison G W, Giglio R F, Batich C D, Berry C R, Case J B and Kim S E 2018 Gradual attenuation of a congenital extrahepatic portosystemic shunt with a self-retaining polyacrylic acid-silicone device in 6 dogs *Vet. Surg.* **47** 722–8

[38] Kalakkunnath S, Kalika D S, Lin H, Raharjo R D and Freeman B D 2007 Molecular relaxation in cross-linked poly(ethylene glycol) and poly(propylene glycol) diacrylate networks by dielectric spectroscopy *Polymer (Guildf).* **48** 579–89

[39] Wu Y, Park H B, Kai T, Freeman B D and Kalika D S 2010 Water uptake , transport and structure characterization in poly (ethylene glycol) diacrylate hydrogels **347** 197–208

[40] Fan J, Chen J, Yang L, Lin H and Cao F 2009 Preparation of dual-sensitive graft copolymer hydrogel based on N-maleoyl-chitosan and poly(N-isopropylacrylamide) by electron beam radiation *Bull. Mater. Sci.* **32** 521–6

[41] Jovančić P, Vílchez A and Molina R 2016 Synthesis of Thermo-Sensitive Hydrogels from Free Radical Copolymerization of NIPAAm with MBA Initiated by Atmospheric Plasma Treatment *Plasma Process. Polym.* **13** 752–60

[42] Wu S W, Liu X, Miller A L, Cheng Y S, Yeh M L and Lu L 2018 Strengthening

injectable thermo-sensitive NIPAAm-g-chitosan hydrogels using chemical cross-linking of disulfide bonds as scaffolds for tissue engineering *Carbohydr. Polym.* **192** 308–16

[43] Choi E J, Ha S, Lee J, Premkumar T and Song C 2018 UV-mediated synthesis of pNIPAM-crosslinked double-network alginate hydrogels: Enhanced mechanical and shape-memory properties by metal ions and temperature *Polymer (Guildf).* **149** 206–12

[44] Canillas M, Geever T, Vieira K, Nugent M J D, Killion J A, Devine D M and Rodríguez M A 2018 Photopolymerization for filling porous ceramic matrix: Improvement of mechanical properties and drug delivering behavior *Polym. Compos.* **0**

[45] Yang J M and Lin H T 2004 Properties of chitosan containing PP-g-AA-g-NIPAAm bigraft nonwoven fabric for wound dressing **243** 1–7

[46] Farooqi Z H, Khan H U, Shah S M and Siddiq M 2017 Stability of poly(N-isopropylacrylamide-co-acrylic acid) polymer microgels under various conditions of temperature, pH and salt concentration *Arab. J. Chem.* **10** 329–35

[47] Kurecic M, Sfiligoj-Smole M and Stana-Kleinschek K 2012 UV polymerization of poly (N-isopropylacrylamide) hydrogel *Mater. Technol.* **46** 87–91

[48] Jose J, Shehzad F and Al-Harthi M a. 2014 Preparation method and physical, mechanical, thermal characterization of poly(vinyl alcohol)/poly(acrylic acid) blends *Polym. Bull.* **71** 2787–802

[49] Shin M S, Kang H seok, Park T G and Yang J-W 2002 Synthesis and characterization of pH/temperature-sensitive hydrogels based on chitosan derivative *Polym. Bull.* **47** 451–6

[50] Canillas M, De Lima G G, Rodríguez M A, Nugent M J D and Devine D M 2016 Bioactive composites fabricated by freezing-thawing method for bone regeneration applications *J. Polym. Sci. Part B Polym. Phys.* **54** 761–73

[51] Killion J A, Kehoe S, Geever L M, Devine D M, Sheehan E, Boyd D and Higginbotham C L 2013 Hydrogel/bioactive glass composites for bone regeneration applications: Synthesis and characterisation *Mater. Sci. Eng. C* **33**

4203–12

[52] Killion J A, Geever L M, Devine D M and Higginbotham C L 2014 Fabrication and in vitro biological evaluation of photopolymerisable hydroxyapatite hydrogel composites for bone regeneration *J. Biomater. Appl.* **28** 1274–83

[53] Killion J A, Geever L M, Devine D M and Higginbotham C L 2014 Fabrication and in vitro biological evaluation of photopolymerisable hydroxyapatite hydrogel composites for bone regeneration *J. Biomater. Appl.* **28** 1274–83

[54] Ortega A M, Kasprzak S E, Yakacki C M, Diani J, Greenberg A R and Gall K 2008 Structure–property relationships in photopolymerizable polymer networks: Effect of composition on the crosslinked structure and resulting thermomechanical properties of a (meth)acrylate-based system *J. Appl. Polym. Sci.* **110** 1559–72

[55] de Lima G G, Campos L, Junqueira A, Devine D M and Nugent M J D 2015 A novel pH-sensitive ceramic-hydrogel for biomedical applications *Polym. Adv. Technol.* **26** 1439–46

[56] KURATA S, MORISHITA K, KAWASE T and UMEMOTO K 2012 Cytotoxic effects of acrylic acid, methacrylic acid, their corresponding saturated carboxylic acids, HEMA, and hydroquinone on fibroblasts derived from human pulp *Dent. Mater. J.* **31** 219–25

[57] Liu T, Zhang L, Joo D and Sun S-C 2017 NF-κB signaling in inflammation *Signal Transduct. Target. Ther.* **2** 17023

[58] Gupta S C, Sundaram C, Reuter S and Aggarwal B B 2010 Inhibiting NF-κB activation by small molecules as a therapeutic strategy *Biochim. Biophys. Acta - Gene Regul. Mech.* **1799** 775–87

[59] Ambrozova N, Ulrichova J and Galandakova A 2017 Models for the study of skin wound healing. The role of Nrf2 and NF-κB *Biomed. Pap.* **161** 1–13

[60] Park Y R, Sultan M T, Park H J, Lee J M, Ju H W, Lee O J, Lee D J, Kaplan D L and Park C H 2018 NF-κB signaling is key in the wound healing processes of silk fibroin *Acta Biomater.* **67** 183–95